Journal of Catalysis 395 (2021) 246–257

Contents lists available at ScienceDirect

Journal of Catalysis

journal homepage: www.elsevier.com/locate/jcat

Pt nanoparticles encapsulated in CeO_2 over-layers synthesized by controlled reductive treatment to suppress CH_4 formation in high-temperature water-gas shift reaction

Jaeha Lee [a], Chengbin Li [b], Sungsu Kang [a], Jungwon Park [a], Ji Man Kim [c], Do Heui Kim [a,*]

[a] School of Chemical and Biological Engineering, Institute of Chemical Processes, Seoul National University, Seoul 08826, Republic of Korea
[b] State Key Laboratory of Catalysis, Dalian Institute of Chemical Physics, Chinese Academy of Sciences, Dalian 116023, China
[c] Department of Chemistry, Sungkyunkwan University, Suwon 16419, Republic of Korea

ARTICLE INFO

Article history:
Received 21 August 2020
Revised 7 January 2021
Accepted 18 January 2021
Available online 27 January 2021

Keywords:
Pt
CeO_2
Pt encapsulation
Water-gas shift reaction
CH_4 selectivity

ABSTRACT

Pt supported on CeO_2 (Pt/CeO_2) is known to be a good catalyst for the water-gas shift (WGS) reaction. However, Pt catalyzes the methanation reaction as a side reaction, which limits the usefulness of Pt/CeO_2 as a catalyst in the high-temperature (HT) WGS reaction. In this study, Pt nanoparticles (Pt NPs) were encapsulated in CeO_2 over-layers ('Pt in CeO_2') by using controlled reductive treatments to suppress the methanation reaction on Pt NPs. 'Pt in CeO_2' catalyst demonstrated the much lower CH_4 selectivity while showing the same high activity in the HT-WGS reaction compared to the conventional 'Pt on CeO_2' catalyst. Detailed characterizations revealed that the underlying Pt NPs promoted the WGS reaction on thin (<1 nm) CeO_2 over-layers by facilitating the formation of active oxygen vacancies. The present contribution to catalyst modification *via* simple thermal treatments will provide additional way to control metal-support interactions to improve catalytic performance.

1. Introduction

The main purpose of the water-gas shift (WGS) reaction is to produce additional H_2 by converting CO with H_2O in H_2-rich feed ($CO + H_2O = CO_2 + H_2$). High-purity H_2 (free of CO) has many uses: it is used, for example, to produce NH_3 or to operate fuel cells (e.g. proton-exchange membrane (PEM) fuel cells) [1,2]. Industrial-scale WGS reactions proceed in two stages: the high-temperature (HT) WGS reaction (350–500 °C) followed by the low-temperature (LT) WGS reaction (200–250 °C) [1,2]. The HT-WGS reaction takes advantage of the high reaction rate, although it has two major disadvantages. **(i)** The HT-WGS reaction is thermodynamically limited, resulting in incomplete CO conversion [1–3]. For this reason, a LT-WGS reactor must be employed after the HT-WGS reactor [1–3]. The LT-WGS reaction can compensate for the thermodynamic constraints and further reduce the CO concentration below 1 vol% [1–3]. **(ii)** Methanation is significantly promoted as the side reaction ($CO + 3H_2 = CH_4 + H_2O$) during the HT-WGS reaction, leading to the loss of H_2 fuel [4–7]. In particular, since the WGS reaction is exothermic, even if the inlet temperature of the HT-WGS reactor is fixed at 350 °C, the outlet temperature of the HT-WGS reactor may exceed 500 °C [1]. At high temperatures (≥450 °C), the methanation reaction is significantly promoted [4–7]. Since this disadvantage limits the types of catalyst that can be used in the HT-WGS reaction, suppressing the CH_4 formation during the HT-WGS reaction becomes important [5,6,8–11].

Currently, CuO-Cr_2O_3-Fe_2O_3 catalyst is commercially used in the HT-WGS reaction [3]. However, because of the toxicity of Cr, the development of alternative catalysts for the HT-WGS reaction is needed [3]. Platinum/cerium(IV) oxide (Pt/CeO_2) catalysts (or catalysts with similar formulations, such as Pt/CeO_2-TiO_2) have received considerable attention as candidate catalysts in the LT-WGS reaction [12–18]. Atomically dispersed Pt^{2+} species or interfacial regions between Pt nanoparticles (NPs) and CeO_2 have been reported to serve as the active sites in the WGS reaction [12,17,19–21]. It would be meaningful if Pt/CeO_2 catalyst having the high intrinsic activity in the WGS reaction could be used in the high-temperature domain. However, Pt/CeO_2 catalysts have an intrinsic drawback in the HT-WGS reaction because Pt greatly promotes the methanation reaction at high temperatures [4]. Therefore, in order to use Pt/CeO_2 as the catalyst in the HT-WGS reaction, a control is needed to suppress the methanation reaction on Pt [4,22,23]. One intuitive strategy to achieve this goal is to block the exposed Pt on the surface to suppress the methanation reaction at high temperature while preserving high activity toward

* Corresponding author.
E-mail address: dohkim@snu.ac.kr (D.H. Kim).

https://doi.org/10.1016/j.jcat.2021.01.021
0021-9517/

the HT-WGS reaction. Tsang et al. reported that by synthesizing Pt@CeO_2 core-shell catalysts with a Pt core and CeO_2 shell, in which all Pt sites are covered with CeO_2 shells, the methanation reaction on Pt is significantly suppressed while high activity in the HT-WGS reaction is maintained [4,22,23]. The results of Tsang et al. have two important implications. **(i)** Beyond the major role of Pt/CeO_2 as a catalyst in the LT-WGS reaction, Pt/CeO_2 can also be used as the catalyst in the HT-WGS reaction with high activity and selectivity. **(ii)** The metal-support interaction between Pt and CeO_2 can grant catalytic activity to the CeO_2 surface of a Pt@CeO_2 core-shell catalyst to achieve high activity in the HT-WGS reaction even if the Pt is completely protected by the CeO_2 shell [4,22,23].

Although Pt@CeO_2 catalysts suggest a new route for the use of the high-activity Pt/CeO_2 system in the HT-WGS reaction without promoting the methanation side-reaction, the synthetic conditions for Pt@CeO_2 limit its practical use. For example, the micro-emulsion technique used to synthesize Pt@CeO_2 catalysts involves several steps that require sophisticated control mechanisms [4]. In addition, expensive cetyltrimethylammonium bromide (CTAB) is required to synthesize the catalyst with the micro-emulsion technique [4]. Therefore, in this contribution, we tried to prepare a 'Pt in CeO_2' catalyst by applying simple controlled reductive treatments to the 'Pt on CeO_2' catalyst to modify its structure. CeO_2 is known to undergo agglomeration at high temperature (e.g. 800 °C) under the reducing conditions [24], and the CeO_2 over-layers are expected to form on Pt NPs during the process. In this context, we hypothesized that the 'Pt in CeO_2' catalyst for the HT-WGS reaction could be synthesized simply by controlled reductive treatments at high temperature. It is noteworthy that CeO_2-encapsulated Pt catalysts are successfully synthesized by utilizing facile and conventional thermal treatments. We found that the 'Pt in CeO_2' catalyst displayed a comparable CO conversion rate in the HT-WGS reaction to the 'Pt on CeO_2' catalyst, while the methanation reaction was significantly suppressed. The catalytic nature of CeO_2 over-layers in interaction with Pt NPs on the 'Pt in CeO_2' catalyst was also studied in detail by combining CO chemisorption, HAADF-STEM, XRD, XPS, and *in-situ* DRIFTS analysis.

2. Materials and methods

2.1. Catalyst synthesis

CeO_2 (Rhodia) has a surface area of 135 m^2/g. Pt (2 wt%) was impregnated on CeO_2 with the incipient wetness impregnation method with aqueous $Pt(NH_3)_4(NO_3)_2$ solution (Sigma Aldrich, 99.99% grade, metal basis) as a metal precursor at room temperature. After impregnation, the catalysts were dried in an oven at 100 °C for 24 hr. Dried catalysts were oxidized under 15 vol% O_2/N_2 at 500 or 800 °C for 2 hr. For example, Pt(2)/CeO_2 500C indicates that dried Pt(2)/CeO_2 was oxidized at 500 °C. The catalytic structure of Pt(2)/CeO_2 500C was modified using two different methods. In the 1st method, samples were reduced under 10 vol% H_2/N_2 at 500 or 800 °C for 2 hr (R treatment). For example, Pt(2)/CeO_2 800R indicates that Pt(2)/CeO_2 500C was reduced at 800 °C. In the 2nd method, after reduction at 250 °C for 2 hr with 10 vol% H_2/N_2, the sample was treated with N_2 at 800 °C for 2 hr (NC treatment). For example, Pt(2)/CeO_2 800NC indicates that Pt(2)/CeO_2 500C was first reduced at 250 °C and then N_2 treated at 800 °C. Reduced catalysts were stabilized under 1 vol% O_2/N_2 at 35 °C for 24 hr. In all cases, the flow rate was 100 mL/min and the ramping rate was 10 °C/min.

2.2. H_2 temperature programmed reduction (TPR)

H_2-TPR analysis was performed in a BET-CAT-BASIC (BEL Japan Inc.) with a thermal conductivity detector (TCD). The catalysts were treated with a He flow (50 mL/min) at 350 °C for 2 hr prior to analysis. After cooling to room temperature, the catalysts were exposed to 5 vol% H_2/Ar (50 mL/min) for 30 min and heated from room temperature to 900 °C at a heating rate of 2 or 10 °C/min.

2.3. Powder X-ray diffraction (XRD)

XRD patterns were taken with a Rigaku (mode 1 smartlab) diffractometer with Cu Kα radiation (λ = 0.1542 nm). The X-ray voltage and current were 40 kV and 30 mA, respectively. The patterns were collected in a 2θ range from 5 to 90° with a scanning step size of 0.02° at a speed of 2.5°/min.

2.4. Surface area measurement

N_2 adsorption/desorption isotherms were measured on a Micromeritics ASAP 2010 apparatus at the temperature of liquid N_2 (-196 °C). Before analysis, all catalysts were pretreated at 300 °C for 4 hr under a vacuum to remove impurities. The pore size distribution and specific surface area were calculated using the Barrett-Joyner-Halenda (BJH) and Brunauer-Emmett-Teller (BET) methods, respectively.

2.5. CO chemisorption

Pulsed CO chemisorption was performed on a BET-CAT-II (BEL Japan Inc.) at −78 and 50 °C using the experimental procedures put forth by Tanabe et al. [25]. First, 0.05 g of sample was oxidized at 500 °C for 15 min. After purging with He, the sample was reduced at the same temperature for 15 min under a 10 vol% H_2/N_2 flow. After cooling to −78 or 50 °C, CO pulses were introduced until adsorption reached saturation. In addition, static CO chemisorption was performed on CeO_2 500C with a Micromeritics ASAP 2010 following previously reported procedures [24]. Briefly, 0.2 g of sample was reduced at 200, 350, or 500 °C under pure H_2 for 2 hr, and CO chemisorption was performed at 35 °C. The Pt dispersion was estimated from CO chemisorption by assuming 1 to 1 stoichiometry of CO to Pt.

2.6. O_2 chemisorption

Pulsed O_2 chemisorption was performed on a BET-CAT-II (BEL Japan Inc.) at 100 °C. After the reductive treatment at 500 °C with 10 vol% H_2/N_2 for 30 min, samples were purged with He at 500 °C for another 30 min. After cooling the sample temperature to 100 °C, O_2 pulses (5 vol% O_2/He in He flow) were introduced until adsorption reached saturation. 0.05 g of sample was used for the analysis. The amount of O_2 adsorbed on Pt was excluded based on the nominal Pt dispersion estimated from CO chemisorption at −78 °C to measure the amount of O_2 adsorbed on CeO_2. Each Pt atom was assumed to adsorb one O atom (O/Pt = 1.0).

2.7. Diffuse reflectance infrared fourier transform spectroscopy (DRIFTS) study

In-situ DRIFTS experiments were conducted in a diffuse reflectance cell (Praying Mantis, Harrick) installed in a Fourier transform infrared (FT-IR) spectrometer (iS-50, Thermo Fisher Scientific) with an MCT detector. 10 vol% H_2/N_2 or 20 vol% O_2/H_2 or N_2 were used to pretreat the sample at 500 °C for 30 min. After the reductive or oxidative pretreatments, the samples were purged with N_2 for another 30 min at 500 °C. Background spectra were obtained after cooling the sample to the CO adsorption temperature and before CO adsorption. 2 vol% CO/N_2 was used for CO adsorption·H_2O (1.5 μL/min) was added to the sample with the syringe pump.

The total flow rate was maintained at 50 mL/min with N_2 balance gas.

2.8. TEM

High-angle annular dark field-scanning transmission electron microscopy (HAADF-STEM) images were obtained with a JEM-2100F (JEOL) electron microscope equipped with a field emission gun at an accelerating voltage of 200 kV. Bright-field TEM images of the samples were also obtained to precisely distinguish lattice fringes and determine the thickness of the CeO_2 over-layers on Pt NPs. To obtain the size distribution curves of the Pt NPs, ~200Pt NPs from several HAADF-STEM images were counted with ImageJ software. Pt dispersion was estimated from size distribution curves according to the following equation [26]:

$$D(\%) = \frac{115.4}{d_p^{0.81}}$$

where D is Pt dispersion and d_p is the average size of Pt NPs. d_p is calculated as follows:

$$d_p = \left(\frac{\sum nd^3}{\sum nd^{2.19}}\right)^{1.23}$$

Here, d is the diameter of Pt NPs, and n is the number of Pt NPs with diameter d.

2.9. X-ray photoelectron spectroscopy (XPS)

XPS analysis was conducted on an AXIS-HSi (Kratos) instrument with Mg Kα radiation (450 W). The charging effects were corrected with respect to the C 1s binding energy of 284.5 eV and the Ce 4f binding energy (u‴) of 916.7 eV [27]. The spectra were processed using casaXPS. Depth-profiling XPS analysis was conducted on a K-alpha instrument (Thermo VG, U.K.) with monochromated Al X-ray radiation (360 W). XP spectra were collected sequentially after the Ar sputtering treatments. (500 eV, raster size 2 mm × 2 mm). The chemical compositions were calculated using the integral intensities of lines of each component considering the atomic sensitivity factors [28]. In addition, XPS spectra were measured five times to calculate the standard deviation of Pt-to-Ce molar ratio.

2.10. Catalytic activity evaluation

The HT-WGS reaction was performed in a fixed bed reactor at atmospheric pressure with 0.06 g of catalyst. The feed mixtures were prepared using mass flow controllers (MKS Instruments, Inc.). The reaction was conducted at 450 °C with **(i)** simple feed containing 3 vol% CO and 24 vol% H_2O or **(ii)** full feed containing 3 vol% CO, 24 vol% H_2O, 3 vol% CO_2, and 20 vol% H_2. The WGS reaction was also conducted at 200 °C with simple feed or full feed to compare the catalytic activities under the differential reaction condition (at CO conversion < 15%). The total flow rate was 70 mL/min with He as the balance gas. The inlet and outlet gas streams were analyzed online using a TCD and a parallel gas chromatograph (GC, Younglin, Inc.) equipped with a Carboxen 1000 column and a flame ionization detector (FID). A methanizer was used to convert CO and CO_2 to CH_4 for quantification by FID. The conversion data were measured when steady-state operation was reached. Before reaction, the catalysts were pretreated with 5 vol% H_2/He at 500 °C for 1 hr. The WGS reaction rate per exposed Pt atom on catalysts was calculated by using the following formula:

$$\text{WGS reaction rate per exposed Pt}\left(\frac{moles\ of\ CO}{moles\ of\ Pt * sec}\right) = \frac{CO\ conversion\ (\%) * CO\ flow\ rate(\frac{mol}{sec})}{Moles\ of\ exposed\ Pt\ on\ catalysts\ (mol)}$$

Here, the moles of exposed Pt on catalysts was estimated from CO chemisorption at −78 °C. In addition, the WGS reaction rate per surface area of catalysts was also calculated to evaluate the WGS activity of the CeO_2 surface of 'Pt in CeO_2' catalysts by using the following formula:

$$\text{WGS reaction rate per surface area of catalysts} \times \left(\frac{moles\ of\ CO}{m^2\ of\ catalysts * sec}\right) = \frac{CO\ conversion\ (\%) * CO\ flow\ rate(\frac{mol}{sec})}{Surface\ area\ of\ catalysts\ (m^2)}$$

Here, the BET surface area of catalysts was used to calculate the WGS reaction rate.

The catalytic stability of Pt(2)/CeO_2 800NC was investigated by performing the WGS reaction at 450 °C for 47 hr under the full feed. Samples were sieved to 150–180 μm size, and 0.05 g of sample was mixed with 0.1 g of α-Al_2O_3. CO conversion and CH_4 yield were estimated by using mass spectroscopy. The total flow rate was 100 mL/min. The selectivity of catalyst for CH_4 during the WGS reaction was also investigated in the temperature range of 400–500 °C. The experimental conditions were the same as those used for the stability test.

3. Results and discussion

3.1. Synthesis of 'Pt in CeO_2' with controlled reductive treatment

As mentioned in Introduction, we tried to cover Pt NPs with CeO_2 over-layers by inducing CeO_2 agglomeration via two controlled reductive treatments (**NC and R methods**). Under oxidizing conditions, Pt forms strong Pt—O—Ce bonds with the CeO_2 surface, which is known to suppress both Pt sintering and CeO_2 agglomeration at high temperature [24,29–31]. Indeed, the crystalline size of CeO_2 in Pt/CeO_2 was smaller than that of CeO_2 after oxidative treatment at 800 °C as evidenced by XRD patterns in Fig. S1. In addition, a high-Pt dispersion was maintained on Pt/CeO_2 800C since an XRD peak corresponding to metallic Pt NPs at 39.5° is not observed in Fig. S1. However, when Pt—O—Ce bonds are reduced (Pt—O—Ce bonds are completely reduced at 250 °C as shown in Fig. S2), both Pt sintering and CeO_2 agglomeration could occur at high temperature (>600 °C) [24]. Hence, Pt(2)/CeO_2 500C was reduced at 250 °C and then treated with N_2 at 800 °C to induce CeO_2 agglomeration (**NC method**). In addition, H_2 treatment at high temperature (>600 °C) accelerates CeO_2 aggregation by reducing CeO_2 bulk. Since the bulk oxygen of CeO_2 is surrounded by Ce atoms, its reduction is thermodynamically unfavorable [29]. For this reason, H_2 can reduce CeO_2 bulk only at temperatures above 600 °C (Fig. S2) [29]. When CeO_2 bulk is reduced at high temperature, vacancies that form in the lattice destabilize the structure of CeO_2 to accelerate CeO_2 aggregation [24]. Thus, Pt(2)/CeO_2 500C was reduced at 800 °C to accelerate CeO_2 agglomeration (**R method**).

To selectively chemisorb CO on Pt and to avoid CO chemisorption on CeO_2, pulsed CO chemisorption was performed at −78 °C after H_2 pretreatment at 500 °C [25]. Fig. 1 and Table S1 display the amount of CO chemisorbed on the Pt(2)/CeO_2 500C, 800R, and 800NC samples. The amount of CO chemisorbed on Pt(2)/CeO_2 500C decreased from 64 to 1 and 5 μmol/g after 800R and 800NC treatments, respectively. Such a huge decrease in CO chemisorption on Pt(2)/CeO_2 after 800R or 800NC treatments might result from either severe Pt sintering or the coverage of Pt

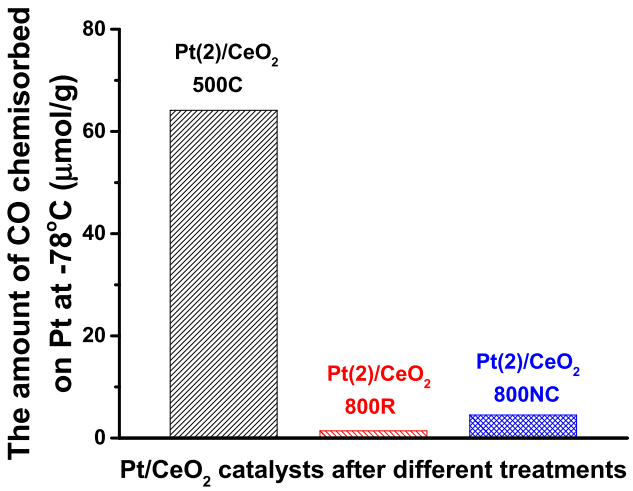

Fig. 1. The amount of CO chemisorbed at −78 °C on Pt(2)/CeO_2 500C, 800R, and 800NC catalysts measured after reductive treatment at 500 °C. CO selectively chemisorbs on Pt at −78 °C (see [25] for details).

NPs with CeO_2 over-layers. According to CO chemisorption results, the nominal Pt dispersion of Pt(2)/CeO_2 500C, 800R, and 800NC samples are 61, 1 and 5%, respectively, which corresponds to the nominal average Pt NP size of 2, 110, and 22 nm, respectively (Table S1). However, no Pt NPs larger than 10 nm were observed in HAADF-STEM images of the Pt(2)/CeO_2 800R (Fig. 2a) and 800NC (Fig. 2b) samples (more HAADF-STEM images are provided in Fig. S3). According to the particle size distribution curves in Fig. 2c obtained from HAADF-STEM images, the average size of Pt NP is 4.0 and 2.4 nm on Pt(2)/CeO_2 800R and Pt(2)/CeO_2 800NC samples, respectively. Note also that the size of Pt NPs on Pt(2)/CeO_2 500C was about 2 nm according to the HAADF-STEM images shown in Fig. S4, which is in fairly good agreement with the CO chemisorption results. The XRD patterns in Fig. S5a also indicate that no large Pt NPs exist in the Pt(2)/CeO_2 800R and 800NC samples, since the intensity of the XRD peak at 39.5° from metallic Pt NPs is small. The Pt dispersions of Pt(2)/CeO_2 800R and 800NC samples, as assessed by CO chemisorption and particle size distribution curves, are compared in Fig. 2d. The Pt dispersions estimated from the Pt size distribution curves were 37 and 56% on Pt(2)/CeO_2 800R and 800NC samples, respectively, which were much higher than those estimated from CO chemisorption, 1 and 5% on Pt(2)/CeO_2 800R and 800NC samples, respectively (Fig. 2d). This indicates that the CeO_2 over-layers deposited on Pt NPs inhibited CO chemisorption on Pt, resulting in underestimation of Pt dispersion of the 'Pt in CeO_2' samples. The combined results imply that the 'Pt in CeO_2' samples were successfully prepared from the 'Pt on CeO_2' sample (Pt(2)/CeO_2 500C) without significant Pt sintering by two different methods (R and NC methods).

According to the Pt NP size distribution curves in Fig. 2c obtained from HAADF-STEM images, all Pt NPs in Pt(2)/CeO_2 800NC were smaller than 5 nm in size, while some Pt NPs in Pt(2)/CeO_2 800R were larger than 5 nm in size. The XRD patterns in Fig. S5b also indicate that a small portion of the Pt NPs in Pt(2)/CeO_2 800R are larger than 5 nm in size. Such a difference could be caused by the more severe change in the structure of Pt/CeO_2 after R treatment than after NC treatment as discussed in the beginning of Section 3.1. Indeed, the XRD patterns in Fig. S5a show that the crystallite size of CeO_2 is 31.1 and 48.4 nm on Pt(2)/CeO_2 800NC and 800R samples, respectively (Table S2). However, it should be stressed that the majority of Pt NPs are around 2 nm in size on both samples (Fig. 2c).

It would be also worth to discuss whether the coverage of Pt NP by CeO_2 over-layers as observed in the present work is related to the Strong-Metal-Support-Interaction (SMSI) phenomena. SMSI phenomena is the reversible loss of the CO adsorption ability of PGM NP supported on reducible oxides after the reductive treatment at high temperature (≥500 °C) [32,33]. Tauster et al. first reported that the CO adsorption ability of Pt/TiO_2 disappeared after the reductive treatment at 500 °C, which recovered after the oxidative treatment at 400 °C [32,34–36]. When oxygen vacancies are formed on reducible oxides, reducible oxides migrate to the surface of PGM NP to minimize the surface energy, resulting in the blockage of CO adsorption sites on PGM NP [37–39]. However, reducible oxides retrieve from the surface of PGM NP when the oxygen vacancies are replenished by the oxidative treatment at high temperature (≥400 °C) to restore the CO adsorption ability of PGM NP [37–39]. To verify whether the suppression of CO adsorption ability after the 800R and 800NC treatments is related to SMSI phenomena, the CO adsorption ability of Pt(2)/CeO_2 800R and 800NC samples were investigated after the oxidative treatment at 400 °C. Table S3 shows that the oxidative treatment at 400 °C has little effect on the CO adsorption abilities of Pt(2)/CeO_2 800R and 800NC samples. Since the suppression of CO adsorption ability is not reversible, the formation of CeO_2 over-layers on Pt NP during the CeO_2 agglomeration is not related to SMSI phenomena. While core-shell synthetic strategies, inverse-catalyst synthetic strategies or SMSI phenomena have been implemented to form metal-oxide over-layers on PGM NP surface [37,40,41], we believe that the present synthetic approach would provide simple alternative to the field.

3.2. Comparison of HT-WGS reaction activity of the 'Pt on CeO_2' and 'Pt in CeO_2' catalysts

In this section, the catalytic performances of CeO_2, 'Pt on CeO_2' and 'Pt in CeO_2' samples in the HT-WGS reaction are comparatively investigated. Table 1 summarizes the HT-WGS reaction activities of high-surface area CeO_2 (135 m^2/g), 'Pt on CeO_2' (Pt(2)/CeO_2 500C) and 'Pt in CeO_2' (Pt(2)/CeO_2 800R and 800NC) catalysts evaluated at 450 °C with simple feed (CO and H_2O) and full feed (CO, H_2O, H_2 and CO_2). Note that CeO_2 and Pt(2)/CeO_2 800R catalysts displayed negligible HT-WGS reaction activity even with the simple feed (Table 1). However, Pt(2)/CeO_2 500C and 800NC catalysts displayed comparable CO conversion during the HT-WGS reaction with both the simple feed and the full feed (Table 1). With the simple feed, the CO conversion during the HT-WGS reaction was 98.1 and 97.1% on Pt(2)/CeO_2 500C and 800NC catalysts, respectively. In addition, with the full feed, the CO conversion during the HT-WGS reaction was 51.7 and 51.1% on Pt(2)/CeO_2 500C and 800NC catalysts, respectively. Note that the addition of H_2 and CO_2 to the reactant feed is well known to decrease CO conversion during the HT-WGS reaction by reaching the thermodynamic limit at high temperature [42,43]. Table 1 also compares the CH_4 yield on 'Pt on CeO_2' (Pt(2)/CeO_2 500C) and 'Pt in CeO_2' (Pt(2)/CeO_2 800NC) catalysts. CH_4 is produced from the reaction between H_2 and CO [7]. For this reason, only a small amount of CH_4 is produced in the simple feed (without H_2 and CO_2) on both Pt(2)/CeO_2 500C and 800NC catalysts (CH_4 yield < 0.5% on both samples, Table 1). However, in the full feed (with the inclusion of H_2 and CO_2), the CH_4 yields on Pt(2)/CeO_2 500C and 800NC catalysts were 8.7 and 0.9%, respectively (Table 1). This corresponds to a selectivity toward CH_4 of 16.8 and 1.4% on Pt(2)/CeO_2 500C and 800NC catalysts during the WGS reaction, respectively. While Pt(2)/CeO_2 500C and 800NC catalysts displayed the comparable CO conversion during the HT-WGS reaction with the full feed, Pt(2)/CeO_2 800NC produced much less amount of CH_4 during the HT-WGS reaction (Table 1). It should be also mentioned that 'Pt in CeO_2' (Pt(2)/CeO_2 800NC) catalyst was non-selective to CH_4 formation during the WGS reaction in the temperature region of 400–500 °C (Fig. 3a). Similar to the Pt@CeO_2 core-

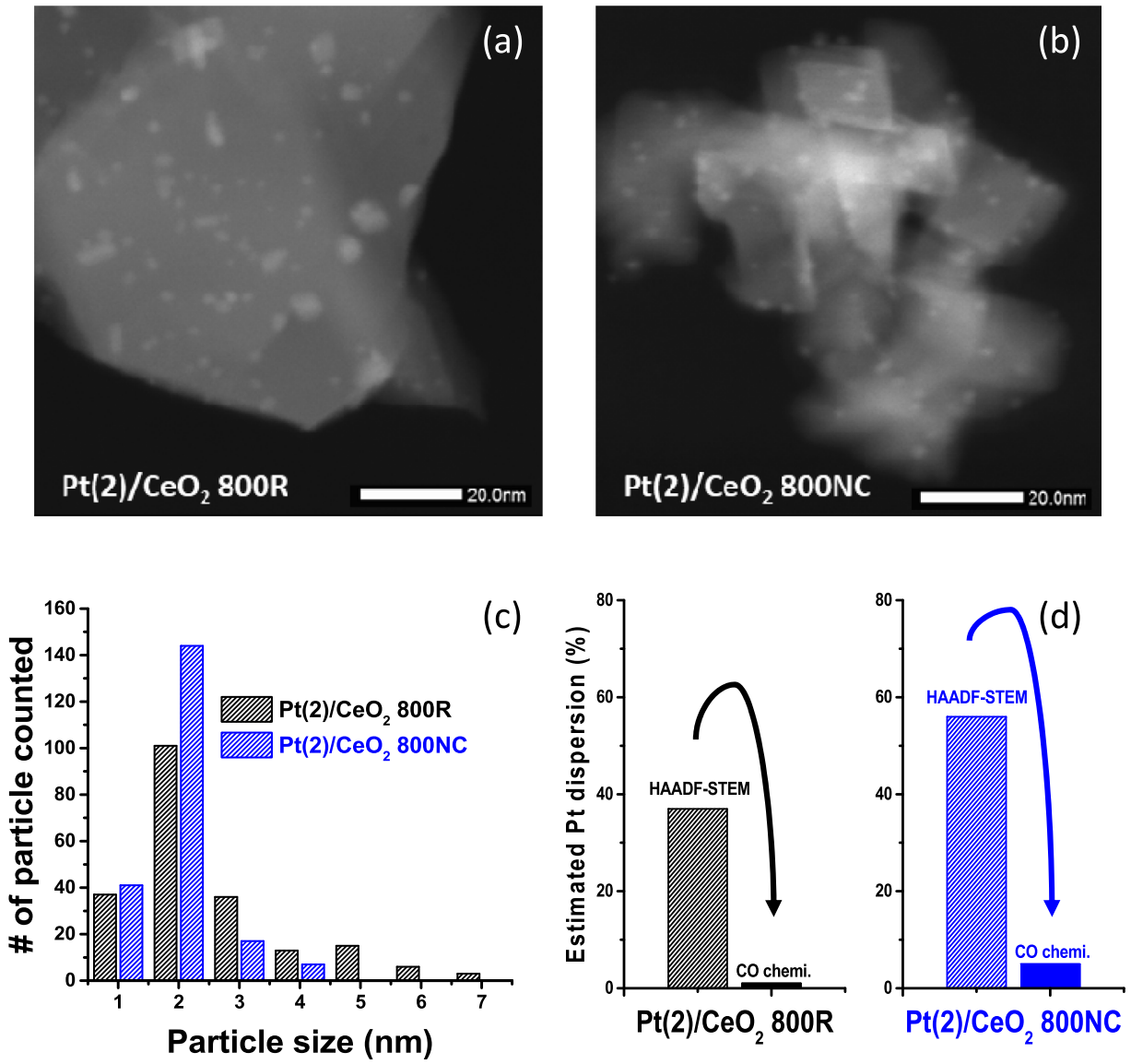

Fig. 2. Representative HAADF-STEM images of Pt(2)/CeO_2 800R (a) and 800NC (b) samples, and (c) their Pt NP size distribution curves. (d) The Pt dispersion of Pt(2)/CeO_2 800R and 800NC samples estimated from CO chemisorption (Fig. 1) and Pt NP particle size distribution curves (Fig. 2c) are compared.

Table 1
HT-WGS reaction activities of CeO_2, Pt(2)/CeO_2 500C, 800R and 800NC catalysts are compared. The reaction was performed at 450 °C under either simple feed (CO + H_2O) or full feed (CO + H_2O + H_2 + CO_2). Catalysts were pretreated with H_2 at 500 °C for 1 hr before evaluating the activity.

Reactant composition	CO + H_2O		CO + H_2O + H_2 + CO_2	
HT-WGS reaction, @450 °C	CO conversion (%)	CH_4 yield (%)	CO conversion (%)	CH_4 yield (%)
Pt(2)/CeO_2 500C ('Pt on CeO_2')	98.1	0.4	51.7	8.7
Pt(2)/CeO_2 800R ('Pt in CeO_2')	3.6	0.0	–	–
Pt(2)/CeO_2 800NC ('Pt in CeO_2')	97.1	0.0	51.1	0.9
CeO_2 (135 m^2/g)	0.4	0.0	–	–

shell catalysts reported by Tsang et al., the CeO_2 over-layers on Pt NPs appear to have suppressed the methanation reaction on Pt NPs during the HT-WGS reaction [4]. The catalytic stability of Pt(2)/CeO_2 800NC was also investigated by performing the HT-WGS reaction at 450 °C for 47 hr under the full feed. Pt(2)/CeO_2 800NC displayed the stable performance, maintaining the equilibrium CO conversion (~51%) throughout 47 hr (Fig. 3b). In addition, the CH_4 yield was only approximately 0.4% during the entire time period, confirming the usefulness of Pt(2)/CeO_2 800NC catalyst (Fig. 3b).

The WGS reaction activities of 'Pt on CeO_2' (Pt(2)/CeO_2 500C) and 'Pt in CeO_2' (Pt(2)/CeO_2 800NC) catalysts were also evaluated at 200 °C to compare the catalytic activity under the differential reaction condition (CO conversion < 15%). Under the simple feed, the CO conversion over 'Pt on CeO_2' and 'Pt in CeO_2' catalysts were 12.7 and 6.1%, respectively (Table 2). On the other hand, under the full feed, the CO conversion over 'Pt on CeO_2' and 'Pt in CeO_2' catalysts were 2.5 and 12.0%, respectively (Table 2). The CO conversion of 'Pt on CeO_2' catalyst decreased from 12.7 to 2.5% when H_2 and CO_2 were added to the feed. The inhibitory effect of H_2 and

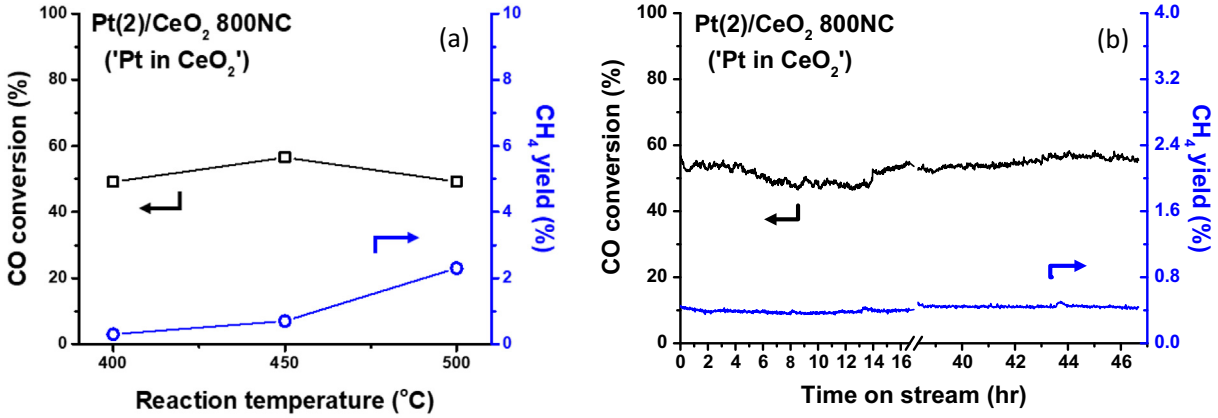

Fig. 3. (a) WGS reaction activities of Pt(2)/CeO_2 800NC ('Pt in CeO_2') catalyst. The reaction was performed at 400, 450 and 500 °C under full feed (CO + H_2O + H_2 + CO_2). Catalysts were pretreated with H_2 at 500 °C for 1 hr before reaction. (b) Catalytic stability of Pt(2)/CeO_2 800NC ('Pt in CeO_2') was examined in terms of CO conversion (left axis) and CH_4 yield (right axis). The WGS reaction was performed at 450 °C under the feed composed of CO, H_2O, CO_2, H_2 and N_2 balance.

CO_2 on the LT-WGS reaction activity of Pt-based catalysts has been reported several times [43–45]. Interestingly, the CO conversion of 'Pt in CeO_2' catalyst increased from 6.1 to 12.0% with the addition of H_2 and CO_2 to the feed. While further study is needed to understand the working chemistry of this phenomenon, the presence of H_2 in the feed may have promoted the catalytic activity of 'Pt in CeO_2' by facilitating the formation of oxygen vacancies on CeO_2 over-layers, which will be discussed in section 3–4.

According to previous reports, the role of Pt in the WGS reaction is to adsorb CO molecules to react with surface hydroxyls on the CeO_2 surface [17,46]. It is interesting that, although Pt is not exposed to reactants on 'Pt in CeO_2' (Pt(2)/CeO_2 800NC) catalyst, it can still catalyze the HT-WGS reaction. It is essential to identify the active sites on 'Pt in CeO_2' catalyst to understand how the HT-WGS reaction can be promoted without producing CH_4; in other words, without exposed Pt sites on the surface. In section 3–3, the WGS reaction activity of 'Pt on CeO_2' (Pt(2)/CeO_2 500C), 'Pt in CeO_2' (Pt(2)/CeO_2 800NC), and CeO_2 samples are comparatively investigated to unravel the change in active sites when 'Pt on CeO_2' catalyst becomes 'Pt in CeO_2' catalyst. In addition, although Pt NPs are covered with CeO_2 over-layers on both Pt(2)/CeO_2 800R and 800NC catalysts, only the latter displayed the activity in the HT-WGS reaction. In section 3–4, Pt(2)/CeO_2 800R and 800NC catalysts are analyzed to understand the factors that determine the catalytic activity of 'Pt in CeO_2'.

3.3. How the interaction between Pt NPs and CeO_2 over-layers influences the catalytic activity of the CeO_2 surface on the 'Pt in CeO_2' catalyst

In-situ DRIFTS experiments could provide useful information to distinguish between different active sites on the 'Pt on CeO_2' and 'Pt in CeO_2' catalysts. The reactivity of CO adsorbed on the 'Pt on CeO_2' (Pt(2)/CeO_2 500C), 'Pt in CeO_2' (Pt(2)/CeO_2 800NC), and CeO_2 samples with H_2O was investigated with *in-situ* DRIFTS analysis. After pretreatment at 500 °C with H_2, CO was adsorbed at 100 °C for 1 hr, followed by N_2 purging at 100 °C for 1 hr to ensure that only strongly adsorbed CO remains on the samples' surface. After that, H_2O was supplied to the sample at 100 °C to react with the adsorbed CO. Note that *in-situ* DRIFTS spectra were collected at 100 °C to prevent the thermal desorption of CO adsorbed on the samples' surfaces at the higher temperature.

After CO adsorption followed by N_2 purging, DRIFTS peaks from monodentate formate were observed on the CeO_2 500C, Pt(2)/CeO_2 500C, and 800NC samples at ~1300 and ~1570 cm^{-1} (Fig. 4) [46]. Additional peak at ~1390 cm^{-1} was observed on Pt(2)/CeO_2 500C. Although the peak at ~1390 cm^{-1} should be related to the O—C—O stretching vibrational mode of carboxyl, bicarbonate or carbonate species [47], the origin of its formation has not been strictly analyzed in the literature (Fig. 4). In the case of CeO_2 500C, CO would adsorb on the CeO_2 surface. On the other hand, on Pt(2)/CeO_2 500C

Table 2
WGS reaction activities of CeO_2, Pt(2)/CeO_2 500C, 800R and 800NC catalysts are compared under the differential reaction condition. The catalytic activity was evaluated at 200 °C under simple feed (CO + H_2O) or full feed (CO + H_2O + H_2 + CO_2). Catalysts were pretreated with H_2 at 500 °C for 1 hr before reaction. Reaction rate was calculated either per exposed Pt on catalyst estimated from CO chemisorption at −78 °C (μmol of CO/μmol of Pt/s) or per BET surface area of catalyst (μmol of CO/m^2 of catalyst/s).

Reactant composition WGS reaction, @200 °C	CO + H_2O				CO + H_2O + H_2 + CO_2			
	CO conversion (%)	Reaction rate		CH_4 yield (%)	CO conversion (%)	Reaction rate		CH_4 yield (%)
		per exposed Pt (μmol of CO/μmol of Pt/s)	per surface area (μmol of CO/m^2 of catalyst/s)			per exposed Pt (μmol of CO/μmol of Pt/s)	per surface area (μmol of CO/m^2 of catalyst/s)	
Pt(2)/CeO_2 500C ('Pt on CeO_2')	12.7	0.05	0.027	0	2.5	0.01	0.005	0
Pt(2)/CeO_2 800R ('Pt in CeO_2')	0.4	0.10	0.006	0	–	–	–	–
Pt(2)/CeO_2 800NC ('Pt in CeO_2')	6.1	0.32	0.048	0	12.0	0.63	0.095	0
CeO_2 (135 m^2/g)	0	0	0	0	–	–	–	–

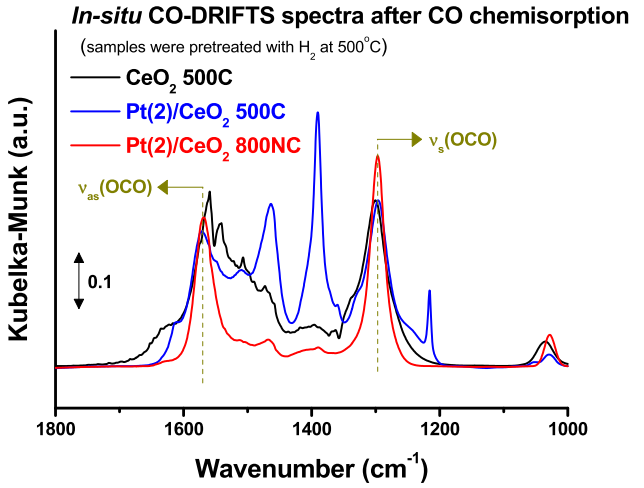

Fig. 4. *In-situ* DRIFTS spectra of CeO_2 500C and Pt(2)/CeO_2 500C and 800NC samples. Samples were pretreated with H_2 at 500 °C for 30 min. After taking the background spectra at 100 °C under N_2, the CO-DRIFTS spectra were collected after CO adsorption at 100 °C for 1 hr followed by N_2 purging at 100 °C for 1 hr.

with 2 nm-sized Pt NPs loaded on the CeO_2 surface (see HAADF-STEM images in Fig. S4), CO could also adsorb on the Pt NPs surface or Pt NP-CeO_2 interfacial regions in addition to the CeO_2 surface. *In-situ* CO-DRIFTS spectra of the CeO_2 500C and Pt(2)/CeO_2 500C samples were collected after CO adsorption at 35 °C for 90 min following pretreatment with H_2 at 500 °C (Fig. S6). The intensities of DRIFTS peaks assigned to monodentate formate at ~1300 and ~1570 cm^{-1} were similar on both samples (Fig. S6). However, the DRIFTS peaks at ~1390, ~2080 and ~1840 cm^{-1} were observed only on Pt(2)/CeO_2 500C (Fig. S6). While the peaks at ~ 2080 and ~1840 cm^{-1} could be assigned to linear-boned CO and bridge-bonded CO on Pt NPs, respectively [48–50], the peak at ~1390 cm^{-1} should be assigned to the O—C—O stretching vibrational mode of carboxyl, bicarbonate or carbonate species that are formed by the adsorption of CO at the interface between Pt NP and CeO_2. Such assignment could explain the absence of the DRIFTS peak at ~1390 cm^{-1} on the 'Pt in CeO_2' samples (Fig. 4), since the Pt NP-CeO_2 interface may not exist on the surface when CeO_2 over-layers fully cover Pt NPs.

The monodentate formate (at ~1300 and ~1570 cm^{-1}) on Pt(2)/CeO_2 500C did not react with H_2O according to the DRIFTS spectra in Fig. 5a. Instead, the intensity of the peak at ~1390 cm^{-1}, assigned to the O—C—O stretching vibrational mode of carboxyl, bicarbonate or carbonate species formed by the adsorption of CO at the Pt NP-CeO_2 interface, significantly decreased in intensity upon H_2O exposure (Fig. 5a). At the same time, evolution of CO_2 was observed in the DRIFTS spectra upon H_2O exposure (data not shown). These findings indicate that CO adsorbed on the Pt NP-CeO_2 interfacial regions reacted with H_2O actively to produce CO_2. This agrees with previous reports that Pt NP-CeO_2 interfacial regions catalyze the WGS reaction [17,46]. The DRIFTS peaks from monodentate formate on CeO_2 500C changed only slightly in intensity upon H_2O exposure, which indicates that adsorbed CO on CeO_2 did not react with H_2O (Fig. 5b). On the other hand, the DRIFTS peak intensity from monodentate formate on Pt(2)/CeO_2 800NC decreased gradually upon H_2O exposure (Fig. 5c). In addition, the production of CO_2 was confirmed in the DRIFTS spectra upon H_2O exposure (data not shown). These results indicate that monodentate formate on Pt(2)/CeO_2 800NC actually reacted with H_2O, although this was not the case on Pt(2)/CeO_2 500C or CeO_2 500C. Time-on-stream variations in peak intensity of monodentate formate (υ_s(OCO) at ~1300 cm^{-1}) were followed when the feed containing H_2O was introduced. Fig. 5d clearly demonstrates that only the monodentate formate on Pt(2)/CeO_2 800NC reacted with H_2O, while that on CeO_2 500C or Pt(2)/CeO_2 500C did not. This indicates that the active sites for the WGS reaction would be different on the Pt(2)/CeO_2 500C and 800NC catalysts. On Pt(2)/CeO_2 500C, where 2 nm-sized Pt NP is present on the CeO_2 surface, Pt NP-CeO_2 interfacial regions catalyzed the WGS reaction, in agreement with previous reports [17,46,51–53]. On the other hand, on Pt(2)/CeO_2 800NC, where 2 nm-sized Pt NP was covered with CeO_2 over-layers, CeO_2 surface catalyzed the WGS reaction. Since the monodentate formate on CeO_2 500C did not react with H_2O, the interaction between Pt NPs and the CeO_2 surface is expected to grant the catalytic activity to the CeO_2 over-layers on Pt NPs in 'Pt in CeO_2' (Pt(2)/CeO_2 800NC) catalyst.

Caution should be taken in generalizing the conclusions from Fig. 5, since the experimental condition used for the *in-situ* CO-DRIFTS study is different from the actual reaction conditions. However, it is worth mentioning that the conclusions from Fig. 5 are quite consistent with those from previously reported *operando* studies. Efstathiou et al. investigated the WGS reaction mechanism of Pt/CeO_2 catalysts (which is practically equivalent to our 'Pt on CeO_2' catalyst) by steady-state isotopic transient kinetic analysis (SSITKA) coupled with *in-situ* DRIFTS experiments, and concluded that formates should not be considered as an important intermediate in the WGS reaction mechanism [47,53]. This agrees with our observation that monodentate formate on 'Pt on CeO_2' catalyst did not react with H_2O (Fig. 5a). Therefore, the enhanced reactivity of monodentate formate on 'Pt in CeO_2' catalyst as observed in Fig. 5c would be the meaningful change. The reactivity of monodentate formate on 'Pt in CeO_2' catalysts evaluated at 100 °C with *in-situ* DRIFTS experiment would differ from that under the practical reaction condition. However, Fig. 5 clearly demonstrate that the reaction path may have changed when 'Pt on CeO_2' catalyst transformed into 'Pt in CeO_2' catalyst by the controlled reductive treatment.

To gain more insight into the active sites on the 'Pt on CeO_2' (Pt(2)/CeO_2 500C) and 'Pt in CeO_2' (Pt(2)/CeO_2 800NC) catalysts, kinetic analysis was performed. The WGS reaction was performed at 150, 200, 250 and 300 °C under the full feed, and the apparent activation energies (E_a) were obtained by assuming the plug flow reactor model (raw data as well as calculation details are provided in Fig. S7, and results are displayed in Fig. 6) [54]. The activation energies were calculated to be 19.2 and 6.5 kcal/mol on the Pt(2)/CeO_2 500C and 800NC catalysts, respectively (Fig. 6). Note that the E_a of Pt(2)/CeO_2 500C estimated in this work (19.2 kcal/mol) is comparable (within 10%) to the values reported in the literature, confirming the validity of the current work [43,47,55,56]. Here, E_a represents the algebraic sum of intrinsic activation energies of elementary steps and heats of adsorption for equilibrium steps, associated with the prevailing reaction mechanism. Therefore, the large difference in E_a between Pt(2)/CeO_2 500C and 800NC catalysts indicates that some critical steps in the WGS reaction mechanism differ on these two catalysts. This is intuitive considering that both CO and H_2O should be activated on the CeO_2 surface of 'Pt in CeO_2' catalyst, unlike the case of 'Pt on CeO_2' catalyst where Pt and CeO_2 could activate CO and H_2O, respectively. Transformation of inert CeO_2 surface into the catalytically active one by the interaction with Pt NP enabled the HT-WGS reaction to proceed without the formation of CH_4 on Pt.

3.4. Why does only Pt(2)/CeO_2 800NC have the activity, and not Pt(2)/CeO_2 800R?

Although Pt NPs are fully covered with CeO_2 over-layers in both Pt(2)/CeO_2 800R and 800NC catalysts, only Pt(2)/CeO_2 800NC was active in the HT-WGS reaction (Table 1). While the CeO_2 surface should catalyze the WGS reaction in 'Pt in CeO_2' catalysts, the dif-

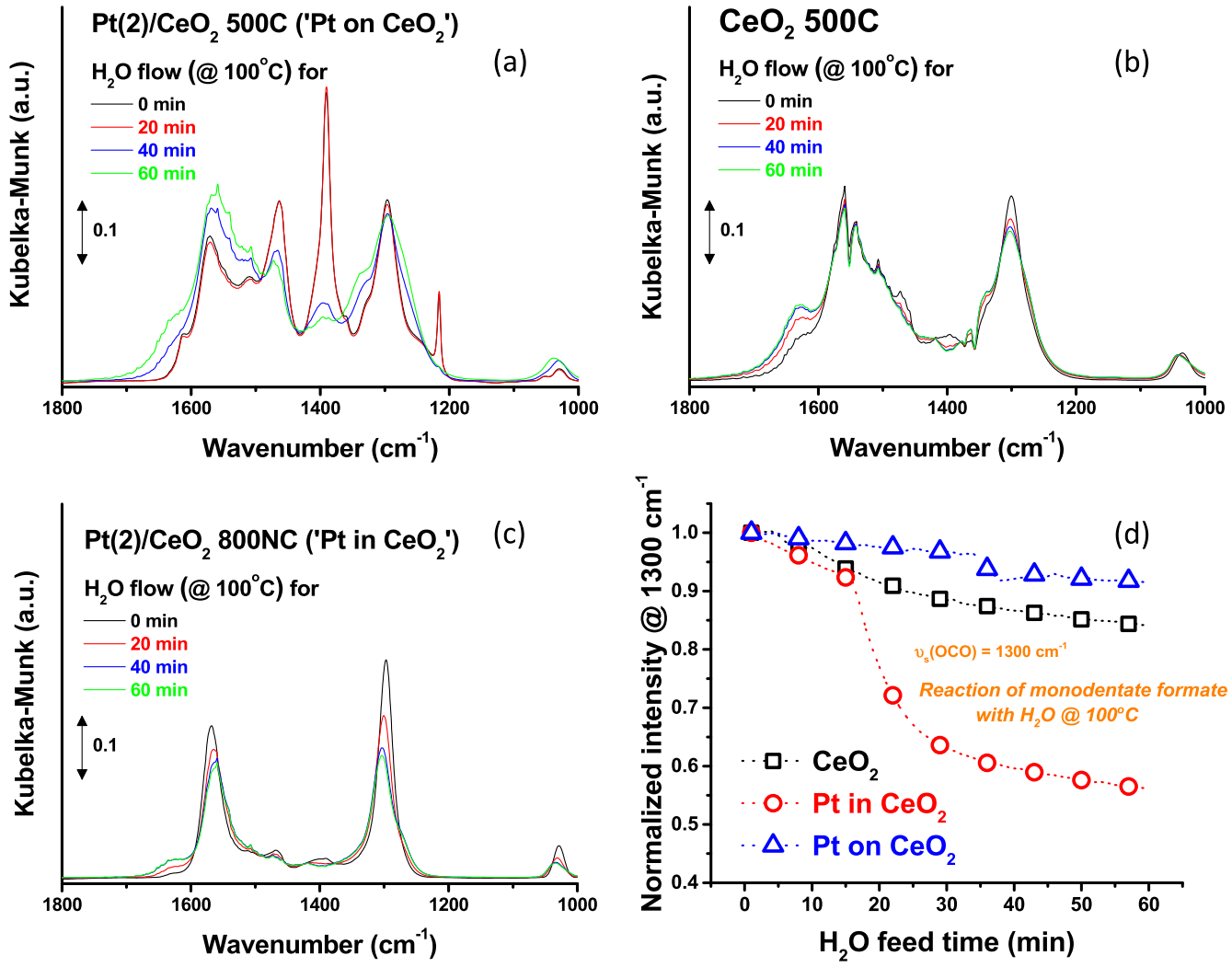

Fig. 5. After CO chemisorption (Fig. 4), *in-situ* DRIFTS spectra were collected while flowing H_2O at 100 °C on (a) Pt(2)/CeO_2 500C, (b) CeO_2 500C, and (c) Pt(2)/CeO_2 800NC samples. (d) The change in intensity of the DRIFTS peak from monodentate formate (υ_s(OCO) at 1300 cm^{-1}) was monitored while flowing H_2O to the samples.

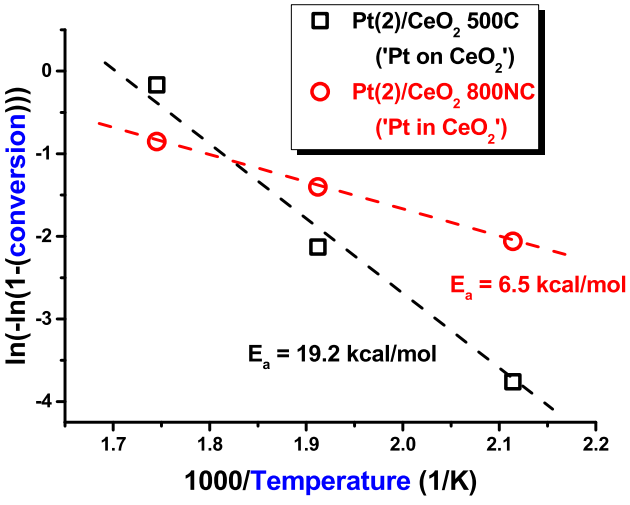

Fig. 6. The activation energies in WGS reaction of the Pt(2)/CeO_2 500C and 800NC catalysts (see Fig. S7 in SI for the detailed derivation).

ference in BET surface area of Pt(2)/CeO_2 800R (17 m^2/g) and 800NC (33 m^2/g) catalysts cannot explain the large difference in the catalytic activity (Table S2). Therefore, the intrinsic catalytic activity of CeO_2 over-layers of Pt(2)/CeO_2 800R and 800NC catalysts would be very different.

To catalyze the WGS reaction, both H_2O and CO should be activated on the catalysts' surface. Here, H_2O can be activated on the oxygen vacancies formed on CeO_2 surface [46,47]. In addition, since 'Pt in CeO_2' catalysts do not expose Pt to the surface, CeO_2 surface should adsorb CO instead of Pt to catalyze the WGS reaction. It can be hypothesized that the presence of oxygen vacancies on CeO_2 surface may alter the CO adsorption ability of CeO_2 surface. The CO adsorption abilities of an oxidized CeO_2 surface and a reduced CeO_2 surface with oxygen vacancies were investigated with static CO chemisorption after the reductive treatments at different temperature (200, 350 and 500 °C). The H_2-TPR spectrum of CeO_2 500C (Fig. S8a) shows that the CeO_2 surface is fully reduced at 500 °C. Some surface reduction occurs at 350 °C, while no reduction occurs at 200 °C. Fig. S8b displays the amount of CO chemisorbed on CeO_2 500C after 200R, 350R, or 500R pretreatments. After 200R treatment, CO chemisorption did not occur. After 350R and 500R treatments, 41 and 133 μmol/g of CO chemisorbed on CeO_2, respectively. Fig. S8 indicates that oxygen vacancies on the reduced CeO_2 surface facilitate CO chemisorption [24]. The role of oxygen vacancies in promoting CO chemisorption was also verified by the *in-situ* CO-DRIFTS spectra of CeO_2 500C (Fig. S9), which was obtained by adsorbing CO at 35 °C for 30 min after pretreat-

ment with H_2 or O_2 at 500 °C. The DRIFTS peak intensities grew much larger after the reductive pretreatment, indicating that oxygen vacancies promoted the CO adsorption on CeO_2 surface (Fig. S9). Hence, oxygen vacancies formed on the CeO_2 over-layers of 'Pt in CeO_2' catalyst would catalyze the WGS reaction by activating both H_2O and CO. Therefore, to understand the difference in the HT-WGS reaction activities of Pt(2)/CeO_2 800R and 800NC catalysts, the concentration of oxygen vacancies on the CeO_2 over-layers of two catalysts should be compared.

In order to quantitatively estimate the concentration of oxygen vacancies formed on CeO_2 over-layers of Pt(2)/CeO_2 800R and 800NC catalysts, O_2 chemisorption was performed at 100 °C. Indeed, the CeO_2 surface of Pt(2)/CeO_2 800NC adsorbs the much larger amount of O_2 than the CeO_2 surface of Pt(2)/CeO_2 800R; CeO_2 of Pt(2)/CeO_2 800R and 800NC catalysts adsorbed 0.3 and 22.6 μmol/g of O_2, respectively, which corresponds to 0.02 and 0.69 μmol/m^2 of O_2, respectively (Fig. 7a). In addition, the O 1s XP spectra in Fig. 7b also indicate a high concentration of oxygen vacancies on Pt(2)/CeO_2 800NC (C 1s, Pt 4f, and Ce 4f XP spectra of the catalysts are provided in Fig. S10.) The XP peak from oxygen vacancies is clearly observed in the region between 529 and 531 eV of Pt(2)/CeO_2 800NC [57–59]. Such a peak was not clearly detected in Pt(2)/CeO_2 500C (not reduced), nor in Pt(2)/CeO_2 800R. Only XP peaks from lattice oxygen (528–530 eV) and surface oxygen or OH groups (531–534 eV) are visible in these samples [57,58]. In summary, both O_2 chemisorption and XP spectra indicate that the concentration of oxygen vacancies formed on CeO_2 over-layers of Pt(2)/CeO_2 800NC is much higher than that formed on CeO_2 over-layers of Pt(2)/CeO_2 800R.

To verify whether the different concentration of oxygen vacancy indeed affects the CO adsorption ability of differently prepared 'Pt in CeO_2' catalysts, the CO adsorption ability of the CeO_2 surface of Pt(2)/CeO_2 800R and 800NC catalysts was evaluated. CO selectively adsorbs on Pt at −78 °C, while CO adsorbs on both Pt and a CeO_2 surface at 50 °C [25]. Hence, the amount of CO adsorbed on the CeO_2 surface of Pt/CeO_2 catalysts could be evaluated by subtracting the amount of CO adsorbed at −78 °C from that adsorbed at 50 °C. Fig. 7c shows that the CeO_2 surface of Pt(2)/CeO_2 800NC (37 μmol/g, or 1.12 μmol/m^2) adsorbs the larger amount of CO than the CeO_2 surface of Pt(2)/CeO_2 800R (12 μmol/g, or 0.70 μmol/m^2). The *in-situ* CO-DRIFTS spectra in Fig. 7d, obtained by adsorbing CO at 100 °C for 90 min after pretreatment with H_2 at 500 °C, also show a larger amount of CO adsorbed on Pt(2)/CeO_2 800NC than on Pt(2)/CeO_2 800R. Fig. 7c and 7d clearly show that the higher concentration of oxygen vacancy on 'Pt in CeO_2' catalyst facilitates the CO adsorption.

Based on the discussion in Fig. 7, it can be speculated that the WGS reaction rate is much higher on Pt(2)/CeO_2 800NC than on

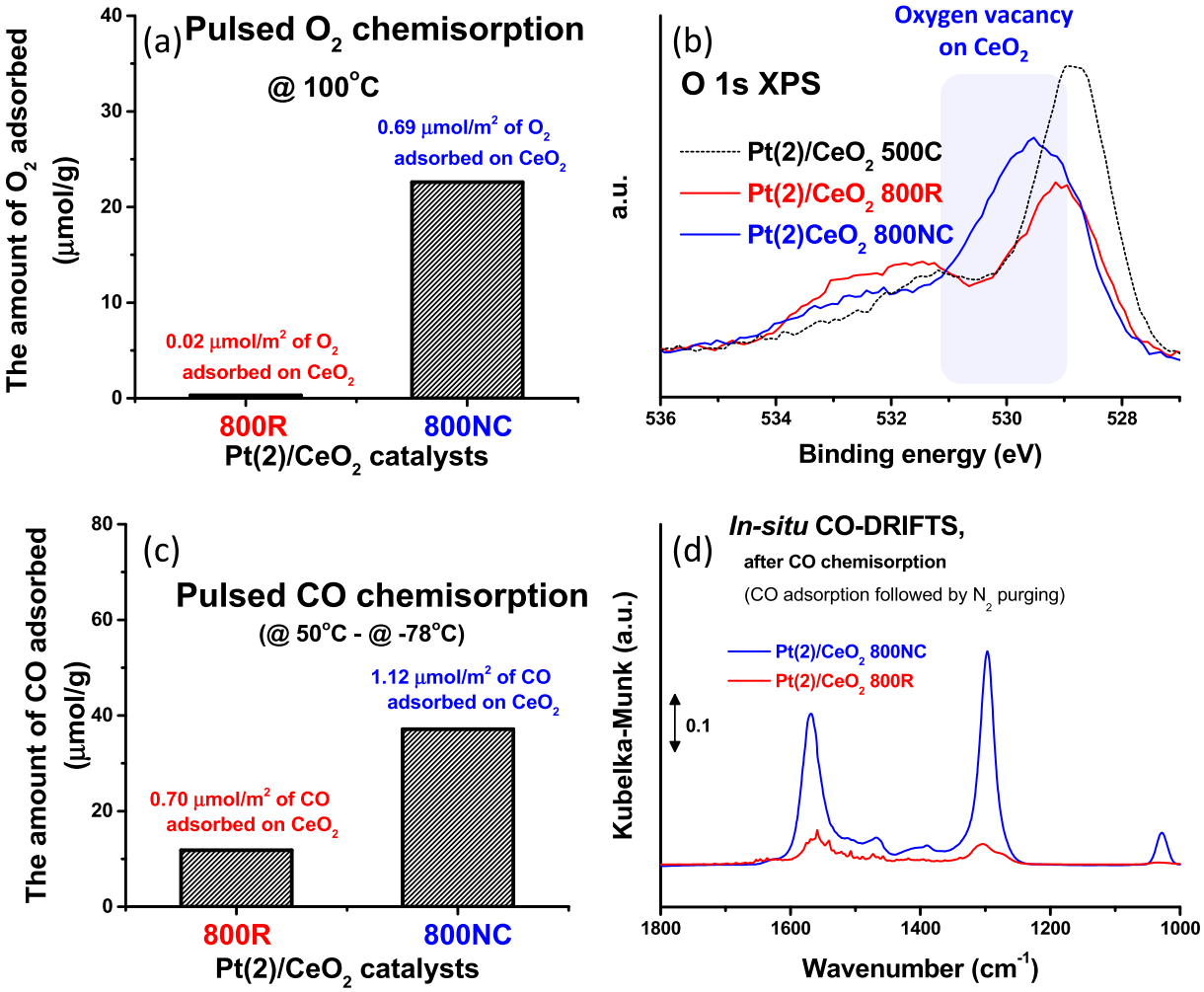

Fig. 7. (a) Pulsed O_2 chemisorption was performed at 100 °C. The amount of O_2 chemisorbed on the CeO_2 surface of each sample is also displayed in the figure. (b) O 1s XP spectra of Pt(2)/CeO_2 500C, 800R, and 800NC samples. (c) Pulsed CO chemisorption was performed at −78 and 50 °C. The amount of CO chemisorbed on the CeO_2 surface of each sample is displayed in the figure. (d) *In-situ* DRIFTS spectra of the Pt(2)/CeO_2 800R and 800NC samples. The samples were pretreated with H_2 at 500 °C. After taking the background spectra at 100 °C under N_2, CO adsorption followed by N_2 purging was performed at 100 °C before collecting the spectra.

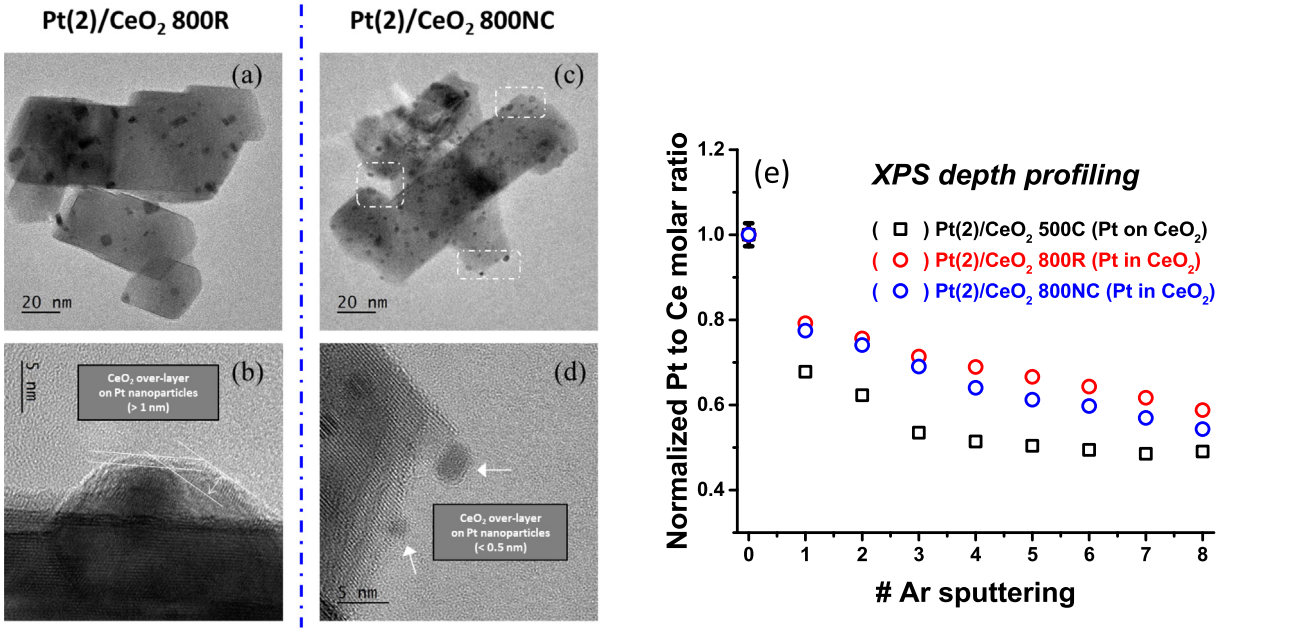

Fig. 8. (a) TEM images of Pt(2)/CeO_2 800R ((a) and (b)) and 800NC ((c) and (d)) samples. (e) Depth-profiling XP spectra of Pt(2)/CeO_2 500C, 800R, and 800NC samples.

Pt(2)/CeO_2 800R (CO conversion, 97.1 vs 3.6% at 450 °C under the simple feed, Table 1), because the former catalyst has the much higher concentration of oxygen vacancy on its CeO_2 over-layers that can activate both CO and H_2O. Analogously to the present work, Hardacre et al. reported that CeO_2 film on a Pt(1 1 1) surface could catalyze CO oxidation reaction, because Pt surface promoted the formation of oxygen vacancies on CeO_2 film [60]. They also suggested that the CeO_2 film should be thin to allow the effective interaction between Pt and CeO_2 to occur [60]. Tsang et al. also reported that the WGS reaction activity of Pt@CeO_2 decreased when the CeO_2 layer became too thick [4]. As we discussed in Section 3.1, structural modification was less severe on Pt(2)/CeO_2 800NC than on Pt(2)/CeO_2 800R. Therefore, the thinner CeO_2 over-layers would have formed on Pt NPs in Pt(2)/CeO_2 800NC than in Pt(2)/CeO_2 800R to possess distinct catalytic activity.

Fig. 8a-d display the bright-field TEM images of Pt(2)/CeO_2 800R and 800NC catalysts. Fig. 8a and b show low- and high- magnification images of Pt(2)/CeO_2 800R, respectively. The CeO_2 over-layers thicker than 1 nm encapsulating Pt NPs could be clearly observed when the periphery of a CeO_2 particle was closely observed (Fig. 8b). Fig. 8c and 8d show low- and high- magnification images of Pt(2)/CeO_2 800NC, respectively. The CeO_2 over-layers thinner than 0.5 nm encapsulating Pt NPs could be clearly observed when the periphery of a CeO_2 particle was closely observed (Fig. 8d) (more TEM images of each sample are provided in Fig. S11). TEM images in Fig. 8a-d strongly indicate that the CeO_2 over-layer is much thicker on Pt(2)/CeO_2 800R than on Pt(2)/CeO_2 800NC.

Fig. 8e displays the depth profiling XP spectra of Pt(2)/CeO_2 500C, 800R, and 800NC samples. The samples were ion sputtered with an Ar gun before each spectrum was taken. Normalized Pt/Ce decreased most rapidly with increasing the number of Ar sputtering in Pt(2)/CeO_2 500C, because Ar could readily remove Pt from 'Pt on CeO_2' sample. On the other hand, normalized Pt/Ce decreased more slowly on 'Pt in CeO_2' samples, which can be explained by the delayed removal of Pt due to the CeO_2 over-layers on Pt NPs (Fig. 8e). In addition, normalized Pt/Ce decreased more slowly on Pt(2)/CeO_2 800R than on Pt(2)/CeO_2 800NC. This is another evidence which indicates that thicker CeO_2 over-layers are formed on the former sample. In summary, although Pt NPs were covered with CeO_2 over-layers after both 800R and 800NC treatments, thinner CeO_2 over-layers are formed on the Pt(2)/CeO_2 800NC. Thin CeO_2 over-layers would interact with Pt NPs to possess the high concentration of oxygen vacancies necessary to catalyze the WGS reaction [60]. It would be worth to mention that while the treatment gas condition determined the thickness of CeO_2 over-layers on Pt NP in this study, the treatment temperature or the surface concentration of Pt (that is, Pt loading) could also influence the thickness of CeO_2 over-layers on Pt NP.

As the last remark, it should be emphasized that the catalytic activities of oxygen vacancies formed on CeO_2 and 'Pt in CeO_2' samples would be completely different. Fig. 9 compares the amount of O_2 chemisorbed at 100 °C after the reductive pretreatment at 500 °C (that would represent the amount of oxygen vacancies

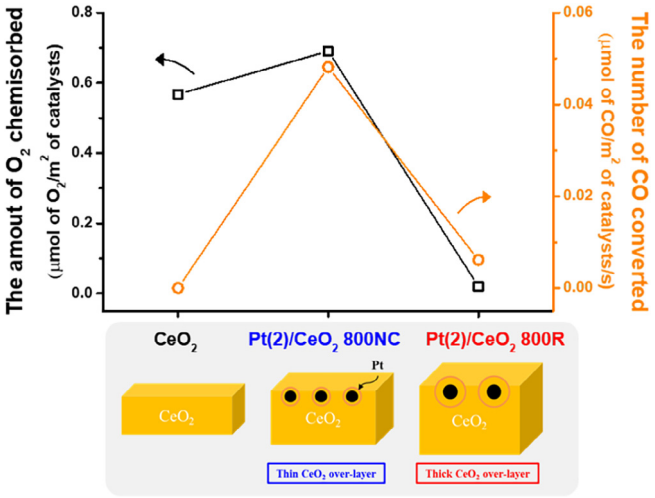

Fig. 9. The amount of O_2 chemisorbed at 100 °C (unit: μmol of O_2/m^2 of catalyst), which would represent the amount of oxygen vacancies formed, is compared to the number of CO converted under the simple feed at 200 °C (data from Table 2, unit: μmol of CO/m^2 of catalysts/s) on the CeO_2 surface of CeO_2, Pt(2)/CeO_2 800NC and 800R catalysts.

formed on the surface) to the number of CO converted under the simple feed at 200 °C (data from Table 2) on the CeO_2 surface of CeO_2 and 'Pt in CeO_2' (Pt(2)/CeO_2 800NC and 800R) catalysts. The amount of O_2 chemisorbed on CeO_2, Pt(2)/CeO_2 800NC and 800R catalysts are 0.56, 0.69 and 0.02 μmol/m^2, respectively. Meanwhile, the number of CO converted on the CeO_2 surface of CeO_2, Pt(2)/CeO_2 800NC and 800R catalysts are 0, 0.048 and 0.006 μmol/m^2/s, respectively. Although the large amount of oxygen vacancies was formed after the reductive treatment at 500 °C, Pt-free CeO_2 surface could not catalyze the WGS reaction (Fig. 9). Indeed, while the oxygen vacancies enabled the adsorption of CO on CeO_2 surface (Fig. S9), the monodentate formate formed on CeO_2 did not react with H_2O (Fig. 5b). On the contrary, Pt(2)/CeO_2 800NC catalyst with thin CeO_2 over-layers on Pt NP not only chemisorbed the large amount of O_2 (0.69 μmol/m^2) but it also displayed high WGS activity (0.048 μmol/m^2/s) (Fig. 9). In line with such observations, monodentate formate formed on Pt(2)/CeO_2 800NC did react with H_2O (Fig. 5c). Meanwhile, Pt(2)/CeO_2 800R catalyst with thick CeO_2 over-layers on Pt NP chemisorbed only little amount of O_2 (0.02 μmol/m^2), and it also displayed low WGS activity (0.006 μmol/m^2/s) (Fig. 9). Therefore, the high catalytic activity of thin CeO_2 over-layers on Pt NP should be resulting from the unique interaction between thin CeO_2 over-layers and Pt NP. Rodriguez et al. demonstrated in their series of publications that the interface between PGM and CeO_2 has the high catalytic activity in the WGS reaction [15,41,61]. However, it should be stressed that little or no interfaces would exist in 'Pt in CeO_2' catalyst. Instead, the fully covered Pt NPs seem to have promoted the intrinsic activity of CeO_2 over-layers in the WGS reaction through the unique metal-support interaction. Recently, Yan et al. reported that hetero-structured MoO_x/γ-Mo_2N greatly promoted the formation of oxygen vacancies on MoO_x surface to accomplish the high catalytic activity of Pt/γ-Mo_2N catalyst in the LT-WGS reaction [44]. They reported that MoO_x thin layers on γ-Mo_2N exhibit a very small formation energy of oxygen vacancies due to the stress induced by the mismatch of lattices of MoO_3 and γ-Mo_2N [44]. Similarly, the lattice mismatch between thin CeO_2 over-layers and Pt NP would lower the formation energy of oxygen vacancies to grant the high catalytic activity to CeO_2 over-layers.

Various strategies have been devised to tailor the metal-support interactions to improve the catalytic performance in several reactions [37,48,62,63]. In this study, the intrinsic WGS reaction activity of CeO_2 was significantly enhanced by tailoring the metal-support interactions between Pt NPs and CeO_2 over-layers without using complex procedures and expensive structure directing agents. We succeeded in preparing the 'Pt in CeO_2' catalyst with simple thermal treatments that has high activity in the HT-WGS reaction and does not produce CH_4 during the reaction. We believe that the current contribution will broaden the horizon of research into ways to manipulate metal-support interactions to develop better catalysts.

4. Conclusion

'Pt in CeO_2' catalysts were synthesized from 'Pt on CeO_2' catalyst by controlled reductive treatments to suppress the methanation reaction while maintaining high activity in the HT-WGS reaction. The structure of Pt(2)/CeO_2 was modified by two different methods: **1.** reductive treatment to reduce CeO_2 bulk (R treatment) and **2.** reductive treatment at 250 °C followed by thermal treatment with N_2 (NC treatment). The HT-WGS reaction activity of Pt/CeO_2 was completely lost after 800R treatment. However, CO conversion during the HT-WGS reaction with the 'Pt in CeO_2' catalyst prepared by 800NC treatment was comparable to that of the 'Pt on CeO_2' catalyst. More importantly, the methanation reaction during HT-WGS was almost completely suppressed on the 'Pt in CeO_2' catalyst. Detailed HAADF-STEM, XPS, CO chemisorption, and *in-situ* DRIFTS studies indicate that thin CeO_2 over-layers formed by 800NC treatment could catalyze the WGS reaction while thick CeO_2 over-layers formed by 800R treatment could not. Therefore, the 'Pt in CeO_2' catalyst prepared by 800NC treatment in this study would be a good candidate catalyst for the HT-WGS reaction.

Declaration of Competing Interest

The authors declare that they have no known competing financial interests or personal relationships that could have appeared to influence the work reported in this paper.

Acknowledgements

This work was supported by a National Research Foundation of Korea (NRF) grant funded by the Korean government (MSIP) (NRF-2016R1A5A1009592).

Appendix A. Supplementary material

Supplementary data to this article can be found online at https://doi.org/10.1016/j.jcat.2021.01.021.

References

[1] C. Ratnasamy, J.P. Wagner, Water gas shift catalysis, Cat. Rev. - Sci. Eng. 51 (2009) 325–440.
[2] T.L. LeValley, A.R. Richard, M. Fan, The progress in water gas shift and steam reforming hydrogen production technologies–a review, Int. J. Hydrog. Energy 39 (2014) 16983–17000.
[3] M. Zhu, I.E. Wachs, Iron-based catalysts for the high-temperature water–gas shift (HT-WGS) reaction: a review, ACS Catal. 6 (2016) 722–732.
[4] C.M. Yeung, K.M.K. Yu, Q.J. Fu, D. Thompsett, M.I. Petch, S.C. Tsang, Engineering Pt in ceria for a maximum metal− support interaction in catalysis, J. Am. Chem. Soc. 127 (2005) 18010–18011.
[5] M. Ang, U. Oemar, E. Saw, L. Mo, Y. Kathiraser, B. Chia, S. Kawi, Highly active Ni/xNa/CeO_2 catalyst for the water–gas shift reaction: effect of sodium on methane suppression, ACS Catal. 4 (2014) 3237–3248.
[6] E. Saw, U. Oemar, X. Tan, Y. Du, A. Borgna, K. Hidajat, S. Kawi, Bimetallic Ni–Cu catalyst supported on CeO_2 for high-temperature water–gas shift reaction: methane suppression via enhanced CO adsorption, J. Catal. 314 (2014) 32–46.
[7] L. Mendelovici, M. Steinberg, Methanation and water-gas shift reactions over $PtCeO_2$, J. Catal. 96 (1985) 285–287.
[8] P. Hongmanorom, J. Ashok, S. Das, N. Dewangan, Z. Bian, G. Mitchell, S. Xi, A. Borgna, S. Kawi, Zr-Ce-incorporated Ni/SBA-15 catalyst for high-temperature water gas shift reaction: methane suppression via incorporated Zr and Ce, J. Catal. (2020).
[9] F. Meshkani, M. Rezaei, Mesoporous Ba-promoted chromium free Fe_2O_3–Al_2O_3–NiO catalyst with low methanation activity for high temperature water gas shift reaction, Catal. Commun. 58 (2015) 26–29.
[10] Y.-L. Lee, A. Jha, W.-J. Jang, J.-O. Shim, C.V. Rode, B.-H. Jeon, J.W. Bae, H.-S. Roh, Effect of alkali and alkaline earth metal on Co/CeO_2 catalyst for the water-gas shift reaction of waste derived synthesis gas, Appl. Catal. A: Gen. 551 (2018) 63–70.
[11] D. Damma, P.G. Smirniotis, Recent advances in iron-based high-temperature water-gas shift catalysis for hydrogen production, Curr. Opin. Chem. Eng. 21 (2018) 103–110.
[12] Q. Fu, H. Saltsburg, M. Flytzani-Stephanopoulos, Active nonmetallic Au and Pt species on ceria-based water-gas shift catalysts, Science 301 (2003) 935–938.
[13] D. Pierre, W. Deng, M. Flytzani-Stephanopoulos, The importance of strongly bound Pt–CeO_x species for the water-gas shift reaction: catalyst activity and stability evaluation, Top. Catal. 46 (2007) 363–373.
[14] G. Jacobs, U.M. Graham, E. Chenu, P.M. Patterson, A. Dozier, B.H. Davis, Low-temperature water–gas shift: impact of Pt promoter loading on the partial reduction of ceria and consequences for catalyst design, J. Catal. 229 (2005) 499–512.
[15] A. Bruix, J.A. Rodriguez, P.J. Ramírez, S.D. Senanayake, J. Evans, J.B. Park, D. Stacchiola, P. Liu, J. Hrbek, F. Illas, A new type of strong metal–support interaction and the production of H_2 through the transformation of water on Pt/CeO_2(111) and Pt/CeO_x/TiO_2(110) catalysts, J. Am. Chem. Soc. 134 (2012) 8968–8974.
[16] L. Pastor-Pérez, V. Belda-Alcázar, C. Marini, M.M. Pastor-Blas, A. Sepúlveda-Escribano, E.V. Ramos-Fernandez, Effect of cold Ar plasma treatment on the catalytic performance of Pt/CeO_2 in water-gas shift reaction (WGS), Appl. Catal. B: Environ. 225 (2018) 121–127.

[17] S. Aranifard, S.C. Ammal, A. Heyden, On the importance of metal–oxide interface sites for the water–gas shift reaction over Pt/CeO_2 catalysts, J. Catal. 309 (2014) 314–324.
[18] T. Montini, M. Melchionna, M. Monai, P. Fornasiero, Fundamentals and catalytic applications of CeO_2-based materials, Chem. Rev. 116 (2016) 5987–6041.
[19] Y. Zhai, D. Pierre, R. Si, W. Deng, P. Ferrin, A.U. Nilekar, G. Peng, J.A. Herron, D.C. Bell, H. Saltsburg, M. Mavrikakis, M. Flytzani-Stephanopoulos, Alkali-stabilized Pt-OH_x species catalyze low-temperature water-gas shift reactions, Science 329 (2010) 1633–1636.
[20] X.-P. Fu, L.-W. Guo, W.-W. Wang, C. Ma, C.-J. Jia, K. Wu, R. Si, L.-D. Sun, C.-H. Yan, Direct identification of active surface species for the water-gas shift reaction on a gold-ceria catalyst, J. Am. Chem. Soc. 141 (2019) 4613–4623.
[21] S.C. Ammal, A. Heyden, Understanding the nature and activity of supported platinum catalysts for the water-gas shift reaction: from metallic nanoclusters to alkali-stabilized single-atom cations, ACS Catal. 9 (2019) 7721–7740.
[22] C.M. Yeung, F. Meunier, R. Burch, D. Thompsett, S.C. Tsang, Comparison of new microemulsion prepared "Pt-in-ceria" catalyst with conventional "Pt-on-ceria" catalyst for water– gas shift reaction, J. Phys. Chem. B 110 (2006) 8540–8543.
[23] C.M.Y. Yeung, S.C. Tsang, Noble metal core– ceria shell catalysts for water–gas shift reaction, J. Phys. Chem. C 113 (2009) 6074–6087.
[24] J. Lee, Y. Ryou, X. Chan, T.J. Kim, D.H. Kim, How Pt interacts with CeO_2 under the reducing and oxidizing environments at elevated temperature: the origin of improved thermal stability of Pt/CeO_2 compared to CeO_2, J. Phys. Chem. C 120 (2016) 25870–25879.
[25] T. Tanabe, Y. Nagai, T. Hirabayashi, N. Takagi, K. Dohmae, N. Takahashi, S.i. Matsumoto, H. Shinjoh, J.N. Kondo, J.C. Schouten, Low temperature CO pulse adsorption for the determination of Pt particle size in a Pt/cerium-based oxide catalyst, Appl. Catal. A: Gen. 370 (2009) 108–113.
[26] A. Borodziński, M. Bonarowska, Relation between crystallite size and dispersion on supported metal catalysts, Langmuir 13 (1997) 5613–5620.
[27] L. Liotta, A. Longo, A. Macaluso, A. Martorana, G. Pantaleo, A. Venezia, G. Deganello, Influence of the SMSI effect on the catalytic activity of a Pt (1%)/$Ce_{0.6}Zr_{0.4}O_2$ catalyst: SAXS, XRD, XPS and TPR investigations, Appl. Catal. B: Environ. 48 (2004) 133–149.
[28] J. Chastain, R.C. King, J. Moulder, Handbook of X-ray Photoelectron Spectroscopy: a Reference Book of Standard Spectra for Identification and Interpretation of XPS Data, Physical Electronics Eden Prairie, MN, 1995.
[29] M. Sanchez, J. Gazquez, Oxygen vacancy model in Strong Metal-Support Interaction, J. Catal. 104 (1987) 120–135.
[30] A. Trovarelli, Catalytic properties of ceria and CeO_2-containing materials, Catal. Rev. 38 (1996) 439–520.
[31] Y. Nagai, T. Hirabayashi, K. Dohmae, N. Takagi, T. Minami, H. Shinjoh, S.i. Matsumoto, Sintering inhibition mechanism of platinum supported on ceria-based oxide and Pt-oxide–support interaction, J. Catal. 242 (2006) 103–109.
[32] S. Tauster, S. Fung, R. Garten, Strong Metal-Support Interactions. Group 8 noble metals supported on titanium dioxide, J. Am. Chem. Soc. 100 (1978) 170–175.
[33] S. Tauster, Strong metal-support interactions, Acc. Chem. Res. 20 (1987) 389–394.
[34] A. Caballero, J.P. Holgado, V.M. Gonzalez-delaCruz, S.E. Habas, T. Herranz, M. Salmeron, In situ spectroscopic detection of SMSI effect in a Ni/CeO_2 system: hydrogen-induced burial and dig out of metallic nickel, Chem. Commun. 46 (2010) 1097–1099.
[35] A. Datye, D. Kalakkad, M. Yao, D.J. Smith, Comparison of metal-support interactions in Pt/TiO_2 and Pt/CeO_2, J. Catal. 155 (1995) 148–153.
[36] S. Bernal, J. Calvino, M. Cauqui, J. Gatica, C. Larese, J.P. Omil, J. Pintado, Some recent results on metal/support interaction effects in NM/CeO_2 (NM: noble metal) catalysts, Catal. Today 50 (1999) 175–206.
[37] I. Ro, J. Resasco, P. Christopher, Approaches for understanding and controlling interfacial effects in oxide-supported metal catalysts, ACS Catal. 8 (2018) 7368–7387.
[38] S. Zhang, P.N. Plessow, J.J. Willis, S. Dai, M. Xu, G.W. Graham, M. Cargnello, F. Abild-Pedersen, X. Pan, Dynamical observation and detailed description of catalysts under strong metal–support interaction, Nano Lett. 16 (2016) 4528–4534.
[39] E.J. Braunschweig, A.D. Logan, A.K. Datye, D.J. Smith, Reversibility of strong metal-support interactions on $RhTiO_2$, J. Catal. 118 (1989) 227–237.
[40] M. Cargnello, P. Fornasiero, R. Gorte, Opportunities for tailoring catalytic properties through metal-support interactions, Catal. Lett. 142 (2012) 1043–1048.
[41] J. Rodriguez, S. Ma, P. Liu, J. Hrbek, J. Evans, M. Perez, Activity of CeO_x and TiO_x nanoparticles grown on Au (111) in the water-gas shift reaction, Science 318 (2007) 1757–1760.
[42] M.G. Castaño, T.R. Reina, S. Ivanova, M. Centeno, J.A. Odriozola, Pt vs. Au in water–gas shift reaction, J. Catal. 314 (2014) 1–9.
[43] G. Germani, Y. Schuurman, Water-gas shift reaction kinetics over μ-structured Pt/CeO_2/Al_2O_3 catalysts, AIChE J. 52 (2006) 1806–1813.
[44] Z.-S. Zhang, Q. Fu, K. Xu, W.-W. Wang, X.-P. Fu, X.-S. Zheng, K. Wu, C. Ma, R. Si, C.-J. Jia, The intrinsically active surface in a Pt/γ-Mo_2N catalyst for the water-gas shift reaction: Molybdenum nitride or molybdenum oxide?, J. Am. Chem. Soc. (2020).
[45] O. Thinon, K. Rachedi, F. Diehl, P. Avenier, Y. Schuurman, Kinetics and mechanism of the water–gas shift reaction over platinum supported catalysts, Top. Catal. 52 (2009) 1940.
[46] J. Vecchietti, A. Bonivardi, W. Xu, D. Stacchiola, J.J. Delgado, M. Calatayud, S.n.E. Collins, Understanding the role of oxygen vacancies in the water gas shift reaction on ceria-supported platinum catalysts, ACS Catal. 4 (2014) 2088–2096.
[47] C.M. Kalamaras, S. Americanou, A.M. Efstathiou, "Redox" vs "associative formate with–OH group regeneration" WGS reaction mechanism on Pt/CeO_2: effect of platinum particle size, J. Catal. 279 (2011) 287–300.
[48] X.I. Pereira-Hernández, A. DeLaRiva, V. Muravev, D. Kunwar, H. Xiong, B. Sudduth, M. Engelhard, L. Kovarik, E.J. Hensen, Y. Wang, Tuning Pt-CeO_2 interactions by high-temperature vapor-phase synthesis for improved reducibility of lattice oxygen, Nat. Commun. 10 (2019) 1358.
[49] J. Resasco, L. DeRita, S. Dai, J.P. Chada, M. Xu, X. Yan, J. Finzel, S. Hanukovich, A. S. Hoffman, G.W. Graham, Uniformity is key in defining structure-function relationships for atomically dispersed metal catalysts: the case of Pt/CeO_2, J. Am. Chem. Soc. 142 (2019) 169–184.
[50] M.J. Kale, P. Christopher, Utilizing quantitative in situ FTIR spectroscopy to identify well-coordinated Pt atoms as the active site for CO oxidation on Al_2O_3-supported Pt catalysts, ACS Catal. 6 (2016) 5599–5609.
[51] C. Kalamaras, D. Dionysiou, A. Efstathiou, Mechanistic Studies of the Water-Gas Shift Reaction over Pt/$Ce_xZr_{1-x}O_2$ Catalysts: The Effect of Pt Particle Size and Zr Dopant, ACS Catal. 2 (2012) 2729–2742.
[52] C.M. Kalamaras, K.C. Petallidou, A.M. Efstathiou, The effect of La_{3+}-doping of CeO_2 support on the water-gas shift reaction mechanism and kinetics over Pt/$Ce_{1-x}La_xO_{2-\delta}$, Appl. Catal. B: Environ. 136 (2013) 225–238.
[53] A.M. Efstathiou, Elucidation of mechanistic and kinetic aspects of water–gas shift reaction on supported Pt and Au catalysts via transient isotopic techniques, Catalysis 28 (2016) 175–236.
[54] Y. Xi, N.A. Ottinger, Z.G. Liu, New insights into sulfur poisoning on a vanadia SCR catalyst under simulated diesel engine operating conditions, Appl. Catal. B: Environ. 160 (2014) 1–9.
[55] M. Yang, J. Liu, S. Lee, B. Zugic, J. Huang, L.F. Allard, M. Flytzani-Stephanopoulos, A common single-site Pt(II)–$O(OH)_x$–species stabilized by sodium on "active" and "inert" supports catalyzes the water-gas shift reaction, J. Am. Chem. Soc. 137 (2015) 3470–3473.
[56] P. Panagiotopoulou, J. Papavasiliou, G. Avgouropoulos, T. Ioannides, D. Kondarides, Water–gas shift activity of doped Pt/CeO_2 catalysts, Chem. Eng. J. 134 (2007) 16–22.
[57] M. Konsolakis, M. Sgourakis, S.A. Carabineiro, Surface and redox properties of cobalt–ceria binary oxides: on the effect of co content and pretreatment conditions, Appl. Surf. Sci. 341 (2015) 48–54.
[58] V. Santos, S. Carabineiro, J. Bakker, O. Soares, X. Chen, M. Pereira, J. Órfão, J. Figueiredo, J. Gascon, F. Kapteijn, Stabilized gold on cerium-modified cryptomelane: highly active in low-temperature CO oxidation, J. Catal. 309 (2014) 58–65.
[59] J.H. Lee, S.H. Lee, J.W. Choung, C.H. Kim, K.-Y. Lee, Ag-incorporated macroporous CeO_2 catalysts for soot oxidation: effects of Ag amount on the generation of active oxygen species, Appl. Catal. B: Environ. 246 (2019) 356–366.
[60] C. Hardacre, R.M. Ormerod, R.M. Lambert, Platinum-promoted catalysis by ceria: a study of carbon monoxide oxidation over Pt (111)/CeO_2, J. Phys. Chem. 98 (1994) 10901–10905.
[61] J.B. Park, J. Graciani, J. Evans, D. Stacchiola, S.D. Senanayake, L. Barrio, P. Liu, J.F. Sanz, J. Hrbek, J.A. Rodriguez, Gold, copper, and platinum nanoparticles dispersed on CeO_x/TiO_2 (110) surfaces: high water-gas shift activity and the nature of the mixed-metal oxide at the nanometer level, J. Am. Chem. Soc. 132 (2010) 356–363.
[62] T.W. van Deelen, C.H. Mejía, K.P. de Jong, Control of metal-support interactions in heterogeneous catalysts to enhance activity and selectivity, Nat. Catal. (2019) 1–16.
[63] J.C. Matsubu, S. Zhang, L. DeRita, N.S. Marinkovic, J.G. Chen, G.W. Graham, X. Pan, P. Christopher, Adsorbate-mediated strong metal–support interactions in oxide-supported Rh catalysts, Nat. Chem. 9 (2017) 120.